EXPERIMENTAL STUDY AND LOCAL APPROACH MODELLING OF DUCTILE DAMAGE IN STEELS OVER A WIDE TEMPERATURE RANGE

A. Hor*, J-L. Lebrun and F. Morel

Arts et Métiers ParisTech, CER Angers, Laboratoire Procédés Matériaux Instrumentation (LMPI),
2 Bd du Ronceray, BP 93525, 49 035 Angers Cedex 1, FRANCE
* *Corresponding author email*: Anis.Hor-7@etudiants.ensam.fr

Keywords: Damage, steel microstructure, experimental techniques, temperature, notched samples, In-situ tensile test.

Abstract. *Several studies [1-2] have been devoted to the identification and modelling of material damage in different forming processes. The aim of this work is to investigate the commonly used local approach models when applied over a wide temperature range. The models investigated include: the Rice-Tracey model [3], the Gurson model [4] and its derivatives, and the Rousselier model [5].*

In the first section the different techniques used to determine the evolution of material damage are discussed. In-situ tensile tests in a Scanning Electron Microscope were used to identify the origin of the appearance of micro-voids as well as their shape. For the 42CrMo4 steel, Magnesium sulphide inclusions are destroyed, leaving room for elliptical voids. A different mechanism is observed in the 100Cr6 steel in which spherical cavities appear in the ferrite phase. In addition, the evolution of the strain fields is determinate using image correlation software (Correli_Q4) [6].

The aim of the second part of this work is to propose changes to the porosity functions of the materials as a function of the strain, degree of triaxiality and temperature. These functions are determined by image analysis of axisymmetrically notched specimens previously deformed under various conditions. The proposed functions are used to extend the above models mentioned above to a wide range of temperatures and strain rates.

1 INTRODUCTION

The modeling of the damage lived much progress these last years, energy approaches [5], based on the homogenization [4] and on the continuous mechanics [7] were developed. However in spite of the evolutions of experimental techniques such as the measurement techniques of kinematic field, the tomography, the microscopy… the comprehension of the damage mechanisms as its evolution at the time of a process especially remains almost unknown when we speak about the thermomechanical processes. The objective of this work is to bring brief replies by various experimental techniques to this question necessary to develop powerful models and nearest possible to reality. The materials used for that are two steels of very close hardness but of different microstructure; the first is 42CrMo4 and the second is 100Cr6 steel.

2 MATERIAL PRESENTATION

The two materials used in the present study are two very close steels of hardness but of different classes; the first is a steel hypo-eutectoid slightly combined with chromium and molybdenum it is the 42CrMo4, its microstructure initial is ferrite-perlite and the second is an hyper-eutectoid slightly combined with chromium it is the 100Cr6, it is presented initially at the state reheated with a ferrite matrix and carbon and chromium carbides not dissolute. An analysis by spectrometry of emission to spark made it possible to determine their chemical compositions which are presented in the tables below:

Element	C	Cr	Mn	Si	Cu	Ni	Mo	S
Concentration (%)	0.40	1.10	0.85	0.23	0.24	0.10	0.20	0.06

Table 1: chemical compositions of 42CrMo4 steel

Element	C	Cr	Mn	Si	Cu	Ni	Mo	S
Concentration (%)	1.03	1.41	0.33	0.24	0.14	0.13	0.02	0.01

Table 2: chemical compositions of 100Cr6 steel

In the same way their microstructures are presented in figure 1. We announce the rather frequent presence of manganese sulphide inclusions in 42CrMo4 steel; these inclusions will play a paramount role in the damage mechanisms of this material:

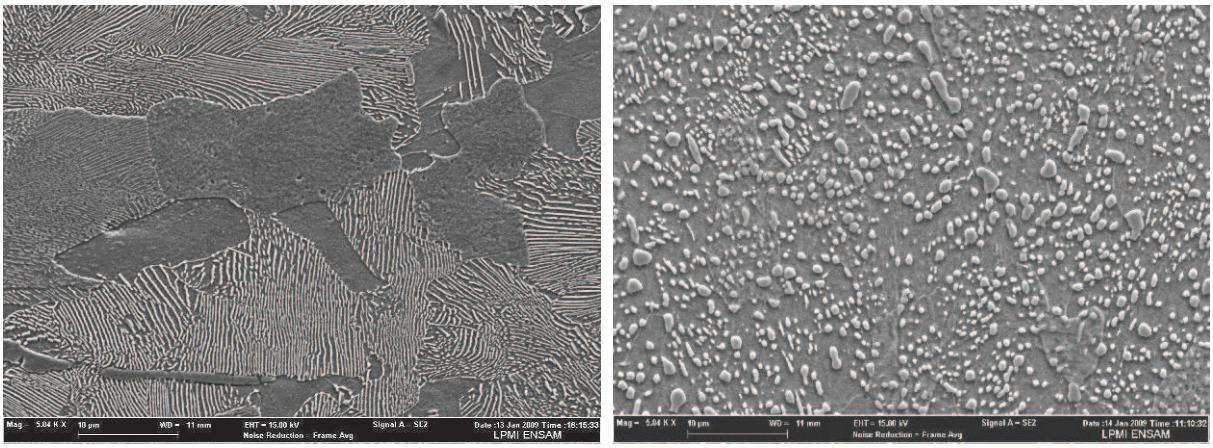

Figure 1 : microstructure of 42CrMo4 steel (hardness:248 HB) on the left and of 100Cr6 steel (hardness:272 HB) on the right

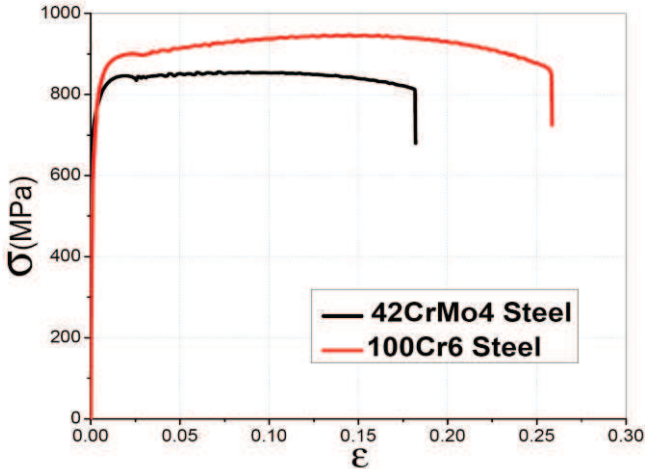

Figure 2 : Cold tensile curve of two studied steels

The cold tensile curves show that the two materials are very ductile. The strain at failure is about 0.18 in the case of the 42CrMo4 steel, which presents a very weak work hardening, and of 0.26 in the case of the 100Cr6 steel whose work hardening is more considerable.¶

3 QUALITATIVE STUDY

The objective of this part is to detect the cold damage mechanisms of two steels and to be able to connect the appearance and the evolution of these mechanisms to the kinetics of the tensile curves.

3.1 Experimental procedure

It is a question of carrying out cold tensile tests inside the SEM. The geometry of the specimens is given by figure 2.The photographs, catches in the center of the test-tube after each step of displacement of 0.01 mm, are treated by digital correlation image software (Correli_Q4). To be able to connect the microstructure to the damage mechanisms, we did not deposit a grid on the specimen. Indeed the specimen polished and are attacked sufficiently to have a contrast allowing the operation of image correlation.

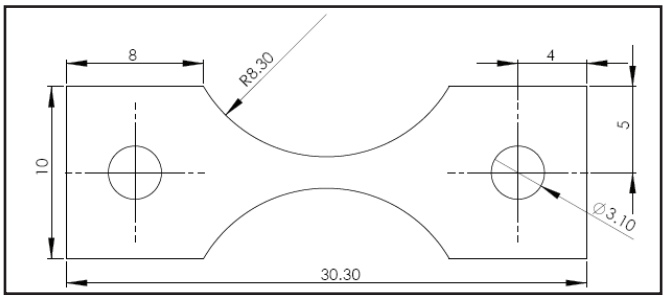

Figure 3: plan of the In-situ tensile specimen

3.2 Some results

The number of the images by tests is relatively high. We chose some photographs by materials to directly illustrate the various phenomena detected either, or after correlation of image. The size in pixel of the elements of the grid corresponding to the image correlation is 8X8 and the photographs size is 1024 X 768 pixels. The error of correlation does not exceed 10^{-2}.

First case: 42CrMo4 steel

- **First example :**

We placed ourselves at a relatively weak enlargement for reasons of texture appropriate to the image correlation. The photographs are taken in the center of the specimen, the direction of tensile is 1 and the equal-values presented in the figure below correspond to the field of deformations ε_{11}.

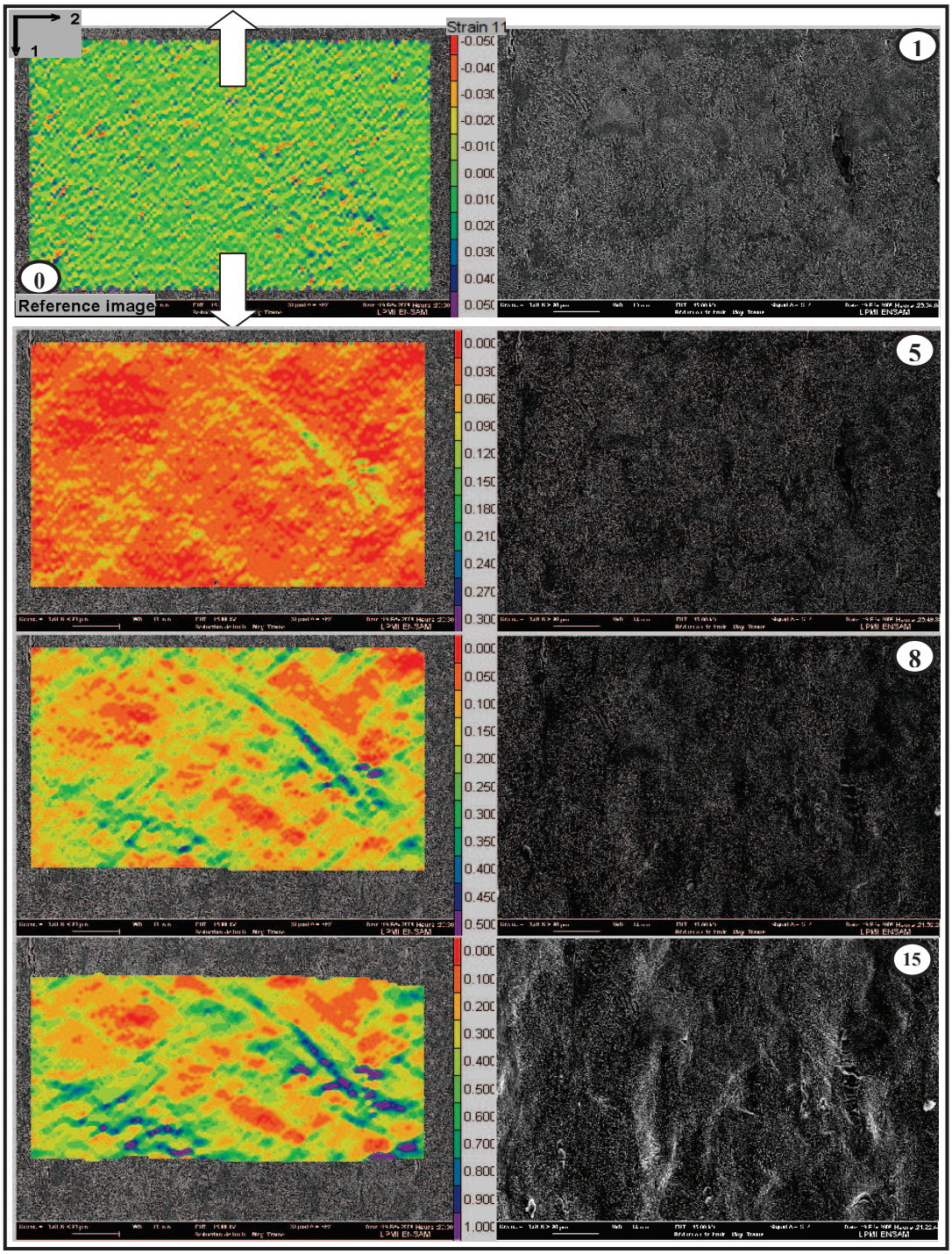

Figure 4: Evolution of the damage in 42CrMo4 steel -Example 1-

- **Second example**

In the first example we saw that the origin of the damage is lengthened manganese sulphide inclusions with their lengthened form. We will discover in this example that in spite of the presence of this type of inclusion, it is an alumina inclusion AlO3with a round form which causes the appearance of cracking.

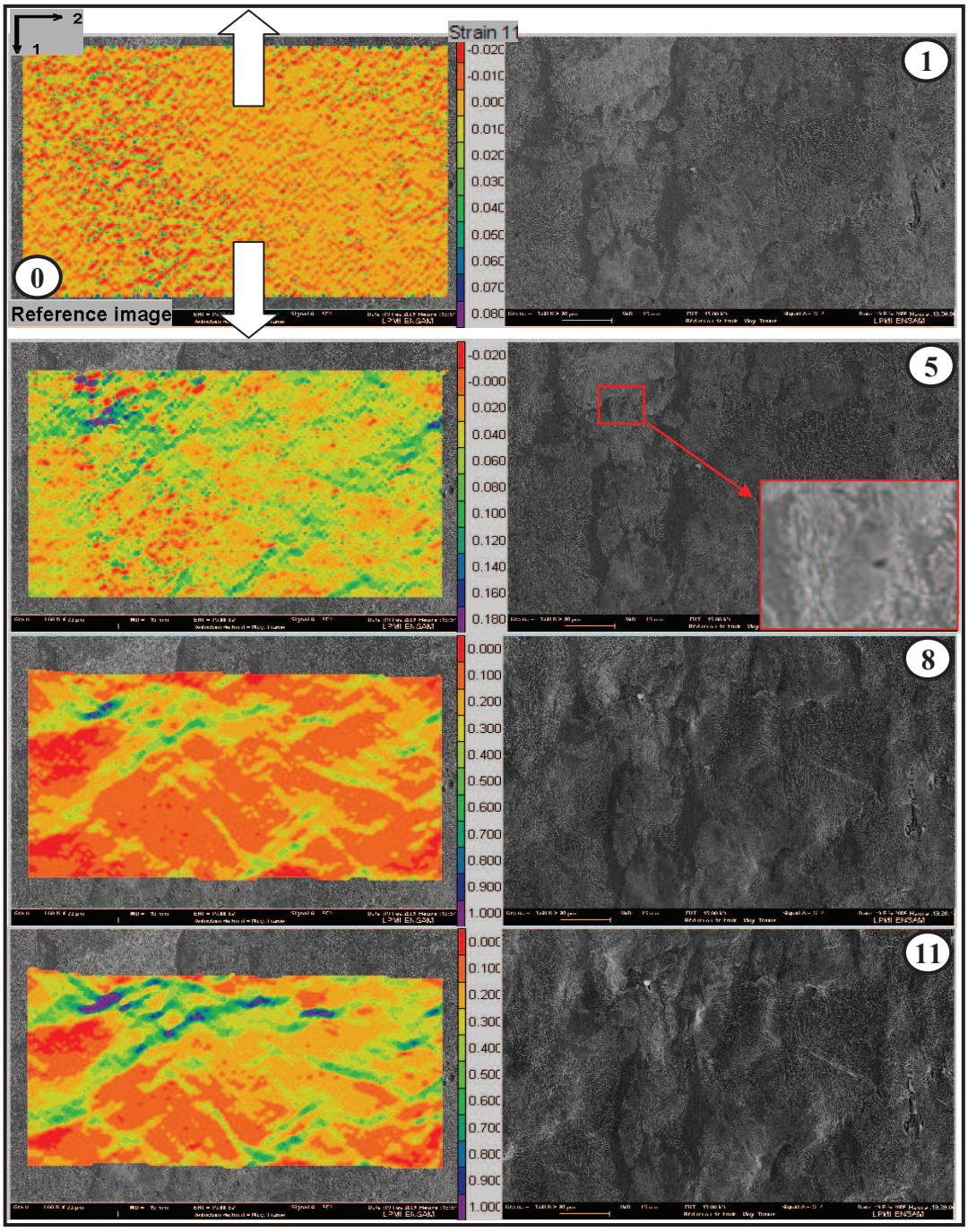

Figure 5: Evolution of the damage in 42CrMo4 steel -Example 2-

<u>Second case: 100Cr6 steel</u>

Contrary to the ferrite-perlite microstructure of the 42CrMo4 steel this does not make it possible to go down on a lower scale. The 100Cr6 steel presents a well textured

microstructure what will able us to have enlargements more raised more clearly to detect the appearance of microporosities.Two scales are presented for this material:

- **First scale :**

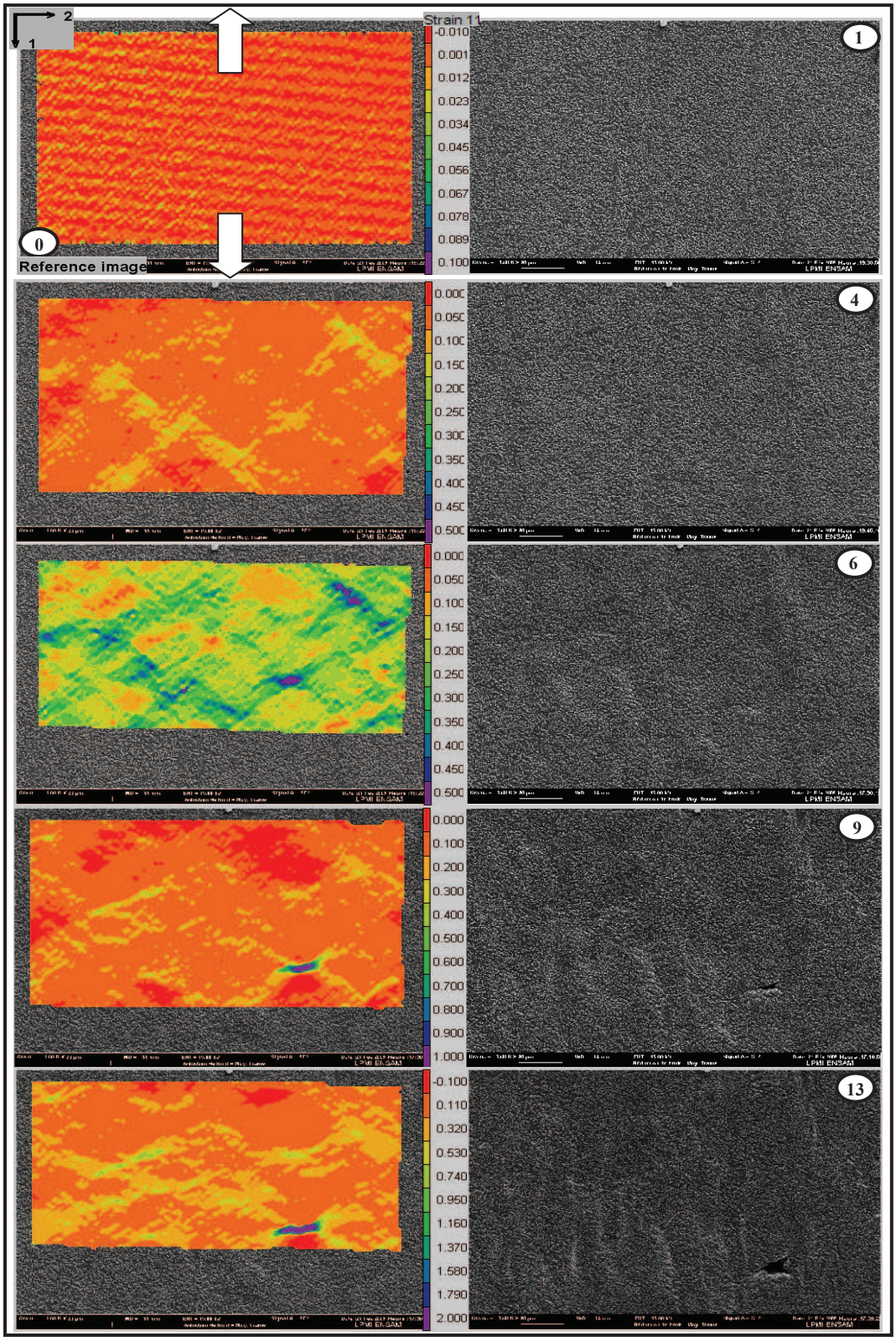

Figure 6: Evolution of the damage in 100Cr6 steel -Example 1-

This example shows us the appearance of porosity but does not give information on the mechanisms causing the appearance of this porosity. For that we will go down on smaller scales.

- **Second scale :**

First example:

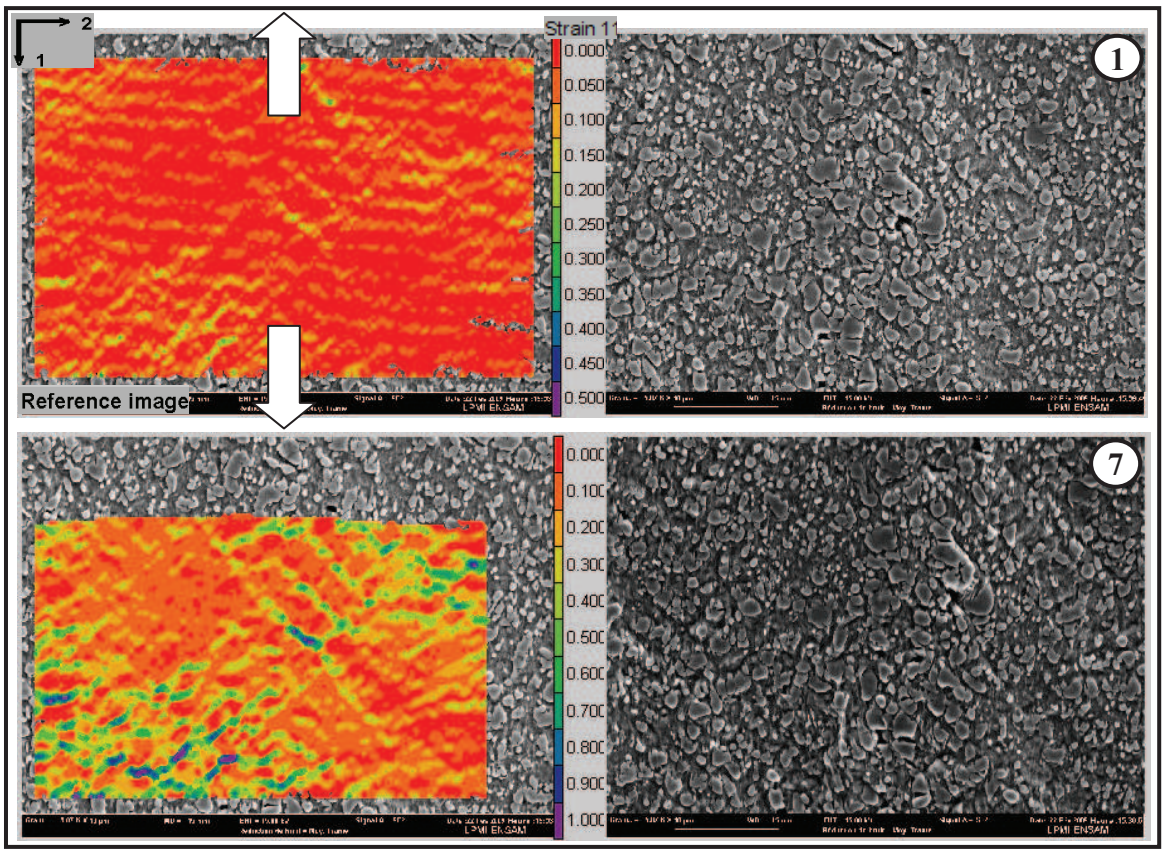

Figure 7: Evolution of the damage in 100Cr6 steel -Example 2-

Second example:

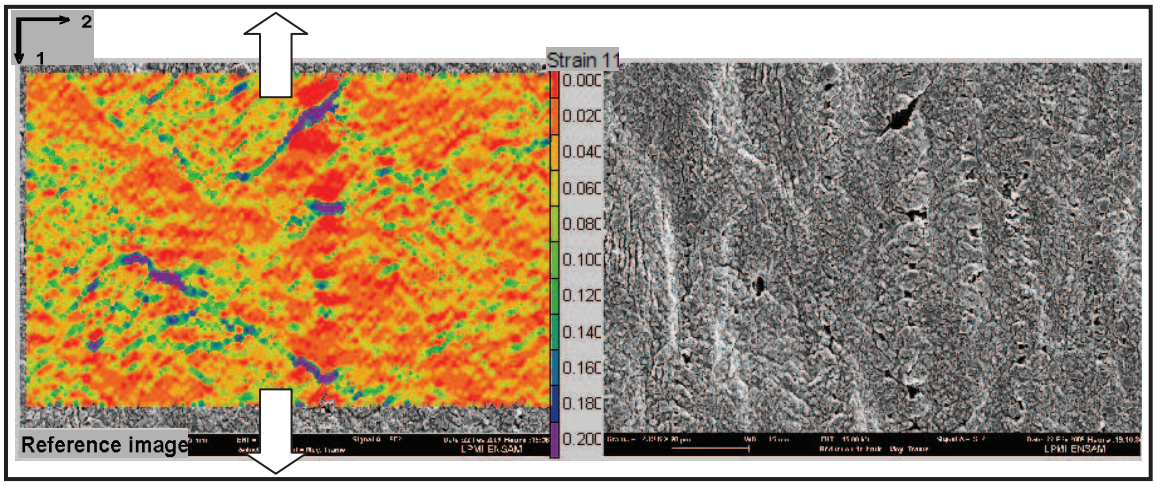

Figure 8 : Evolution of the damage in 100Cr6 steel -Example 3-

3.3 Discussion

In the case of the 42CrMo4 steel, the appearance of the bands of slip late is followed thereafter by breaks to the level of manganese sulphide inclusions. Two cases arise: if the size of inclusion is considerable, the crack starts from this inclusion is propagated while following the joints of the grains. If inclusion is of small size, the crack leaves the grain boundary nearest. We noticed that the very rare presence of alumina inclusions AlO3 (second example) made appearing quickly the crack from where dispersion in the value strain at failure for this material. The phenomena of growth are always the same one for this material on the other hand the phenomenon of coalescence varies according to case's which arises.

In the case of the 100Cr6 steel, the ferrite matrix becomes deformed plastically, the carbides do not adapt what cause the break of these carbides. The breaks develop and starts to meet as of other carbide are breaking them too. The phenomenon of growth and coalescence is the same one for this material what explains the results with a very weak dispersion in the case of this steel. We noticed appearance very early bands of slip this is with the coexistence of a soft and different phase very hard.

We can schematize the damage of two steel in the following way:

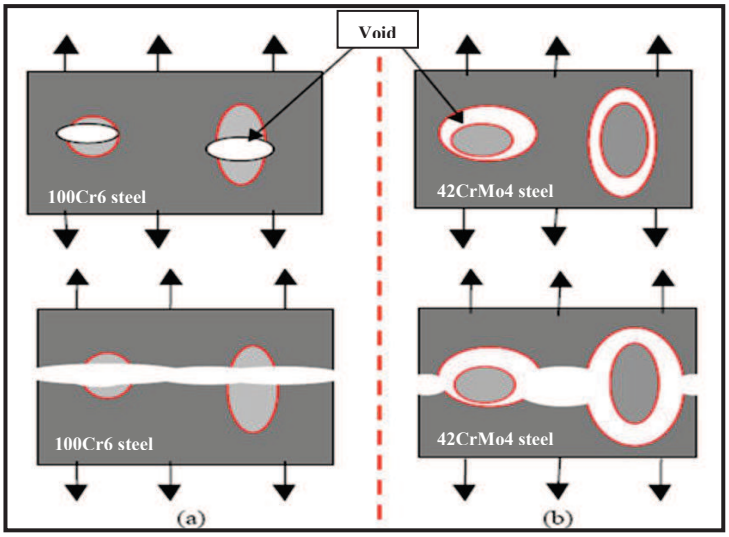

Figure 9: Diagrammatic representation of the two steels damage

4 QUANTITATIVE STUDY

4.1 Experimental procedure

We carried out tensile tests using axisymmetric notched samples (figure 8-A) with various rays of notches. The objective is on the one hand, to determine the strain at failure according the different degree of triaxiality. And other to determine the evolution of porosity according to the plastic deformation by carrying out tests at various strain rates. The tests have were carried out to three temperatures (20C, 400 and 800°C) and at a strain rate of about 10^{-2} s^{-1}.

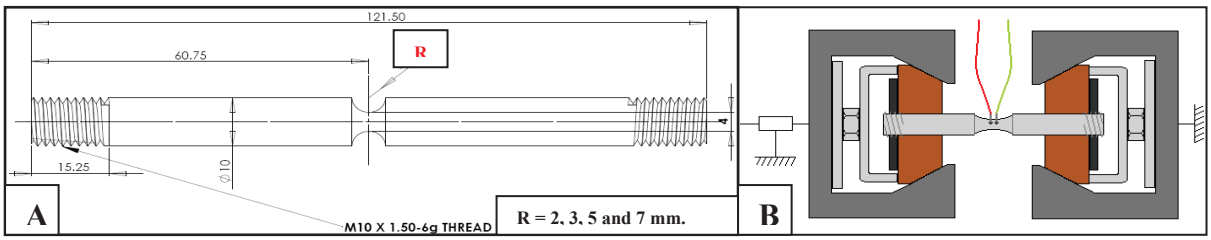

Figure 10: Sample geometry (A), tensile assembly diagram on thermomechanical simulator GLEEBLE 3500 (B)

The method of proportion voids determination consists to cut out the sample in the longitudinal direction, to enrobed, polish and attack them. Automatic acquisition software "MultiScan" makes it possible to sweep a zone in the center of the specimen (figure 11) and to take the images and be able to rebuild the total image of the entire zone. The adequate enlargement to be able to determine the porosity is 5000 and the zone in the center is of 0.5X0.5 mm. The number of the acquired images is approximately 200 photographs. VBA Macro was developed under the image analyze software “VISILOG” to be able to treat the photographs and to calculate the voids volume.

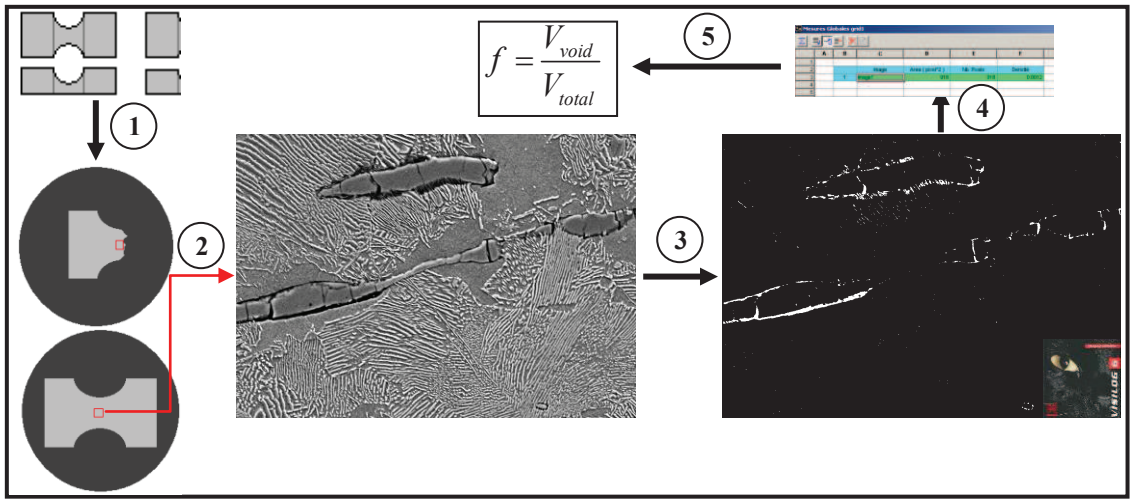

Figure 11: Experimental procedure to determine the porosity fraction

4.2 Triaxiality degree determination

The triaxiality degree is defined as being the relationship between the hydrostatic stress and the equivalent stress:

$$\tau = \frac{\sigma_h}{\sigma_{eq}} = \frac{\frac{1}{3} trace(\boldsymbol{\sigma})}{\sqrt{\frac{3}{2}(\boldsymbol{\sigma}^D : \boldsymbol{\sigma}^D)}} \text{ and, } \boldsymbol{\sigma}^D = \boldsymbol{\sigma} - \frac{1}{3} trace(\boldsymbol{\sigma}).\mathbf{I} \quad (1)$$

An analytical formula in elasticity was given by Bridgman [8]:

$$\tau = \frac{\sigma_h}{\sigma_{eq}} = \frac{1}{3} + Ln(1 + \frac{a}{2R}) \quad (2)$$

a is the diameter at the bottom of the notch, et R is the curvature radius of the notch.

In this paragraph we determine the degree of triaxiality of the various shapes of samples, for that we carried out a numerical simulation on FE code Abaqus Standard using an elastic-plastic behavior law. We kept a constant size of element for all the geometries. The variation of the degree of triaxiality according to the plastic deformation is relatively weak (except worms end because the striction). We are interested in the variation of the degree of triaxiality by moving center of the specimen on the free face at the bottom of the notch.

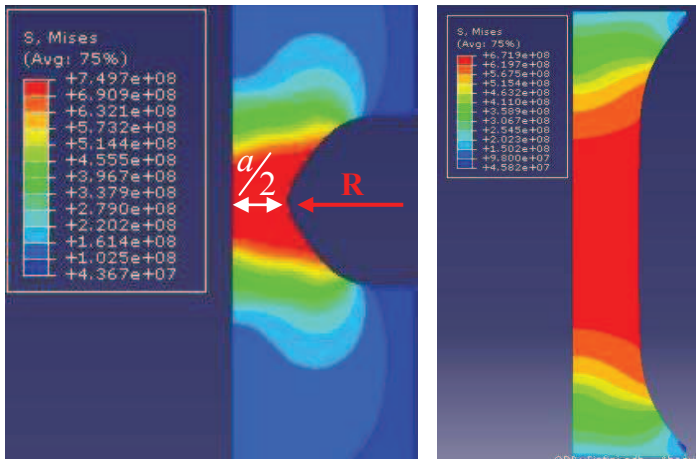

Figure 12: Equivalent stress field in a notched sample on the left and simple specimen on the right

In figure 12 we present the equivalent stress field of Von Mises in the case of a notched sample of ray R and of a simple specimen of useful zone measuring 10 mm. We notice that in the simple specimen the stress field is uniform along this zone where as in the case of the notched sample the field is very heterogeneous. In the continuation, we do not speak any more a true stress. We will introduce the notion of the nominal stress, it is the total effort divided by the critical section:

$$\sigma_n = \frac{Force}{Initial\ Critical\ Section} = \frac{Force}{\pi(a/2)^2} \tag{3}$$

The true strain is not measurable in the case of the notched samples, we use the strain reported to a 10 mm length (it is the distance which separates the two grips of the extensometer). The strain is so equal:

$$\varepsilon_n = Ln(\frac{10+\Delta l}{10}) \tag{4}$$

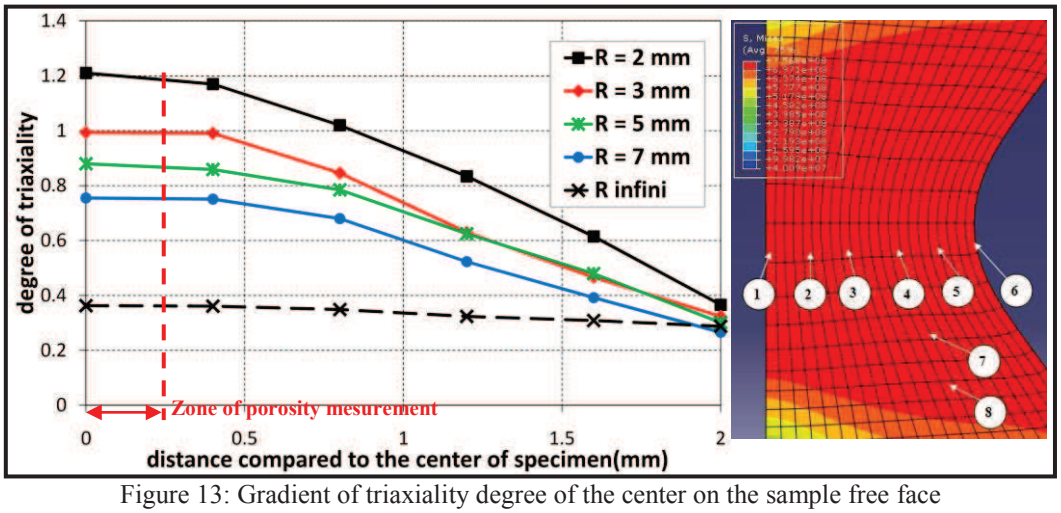

Figure 13: Gradient of triaxiality degree of the center on the sample free face

We note that some of the notch the evolution of the triaxiality degree variation is the same one. Most important to retain that in the zone of evaluation of porosity the triaxiality degree is constant.

4.3 The temperature Heterogeneity

The heating of the specimen is done by electric conduction. It is the passage of the electrical current which causes, according to the resistivity of material, the increase in the temperature. This method of heating introduces the temperature heterogeneities along the sample. The field of temperature can be analytically given in the case of a simple geometry by solving the heat equation:

$$\Delta T = RI^2 = \frac{\rho.L}{S} I^2 \tag{5}$$

L is the sample length, S its section and ρ the material resistivity.
With the boundary conditions:

$$\begin{cases} T(0) = 20\,°C \\ T(L) = 20\,°C \end{cases} \tag{6}$$

In the case of sample with a very low diameter compared to the length, we can add the assumption that $\Delta = \frac{\partial^2}{\partial x^2}$.

The profile of the temperature along the sample follows a parabola whose top is the point (*L/2*, *Timposed*) and the ends are the items (0, 20C) and (*L*, 20C). To decrease the errors according the temperature heterogeneity, it is necessary that the top of the parabola is broad.

In the case of the notched samples the sharp variation of the section increases the degree of temperature heterogeneity. We carried out experimental measurements. A thermoelectric simulation will be carried out thereafter on FE code Abaqus.

It is a question of measuring the temperature in 3 different emplacements from the sample. For that we carried out a thermal cycle which consists to increase the temperature with heat rate 100 °C/s, maintenance during 20 s then cooling with the free vacuum. We also welded 3 thermocouples onto the specimen; the thermocouple in the center is that which controls the temperature instruction and two other measurements only. The results presented below correspond to the case of steel 100Cr6:

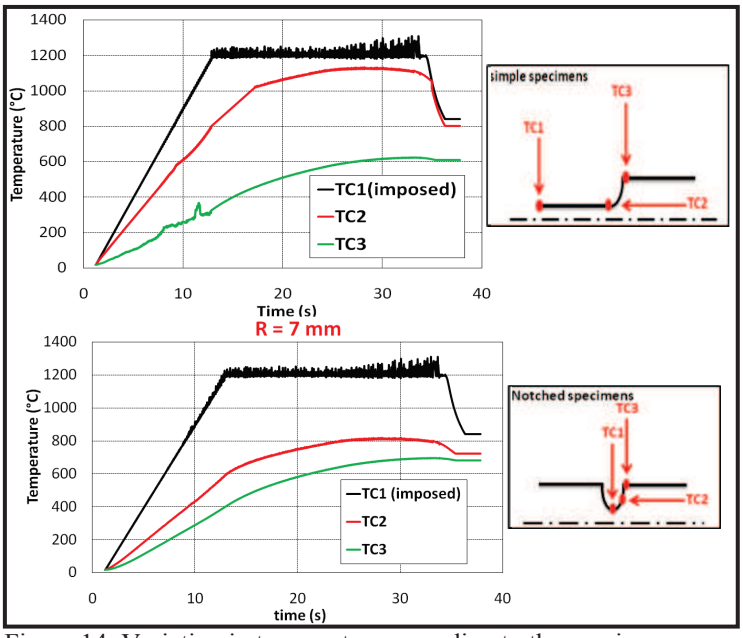

Figure 14: Variation in temperature according to the specimen geometry

The variation in temperature is weak in the useful zone of simple specimen. Nevertheless in the case of the notched samples, we indeed notice a very strong heterogeneity between the bottom of the notch and semi-ray there is a variation of 400 °C on a temperature of 1200 °C.

4.4 Determination of porosity evolution on a wide range of temperature

We present in this paragraph the porosity evolution according to the plastic strain at various temperatures. These results were obtained by the technique of image analysis described previously. We suppose that the material does not present an initial cavity.

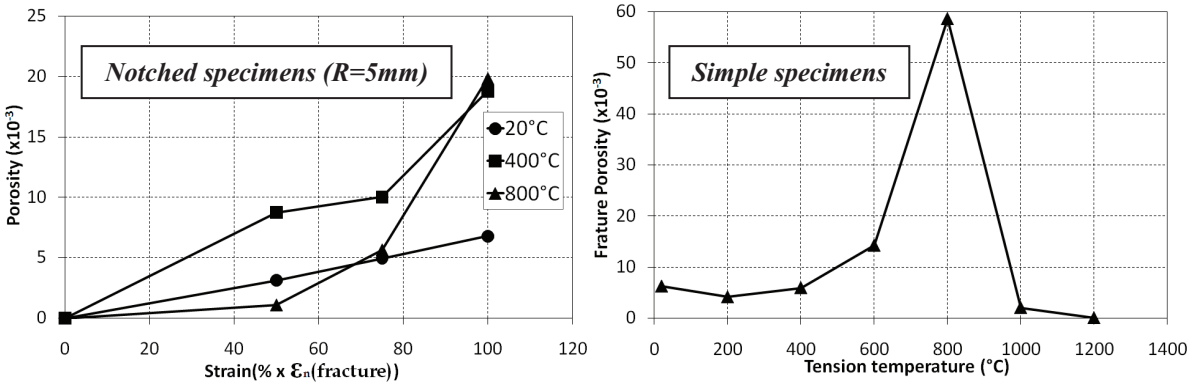

Figure 15: Porosity evolution according to the plastic strain at different temperature (on the left) and the failure porosity according to the temperature (on the right) in the case of 42CrMo4 steel

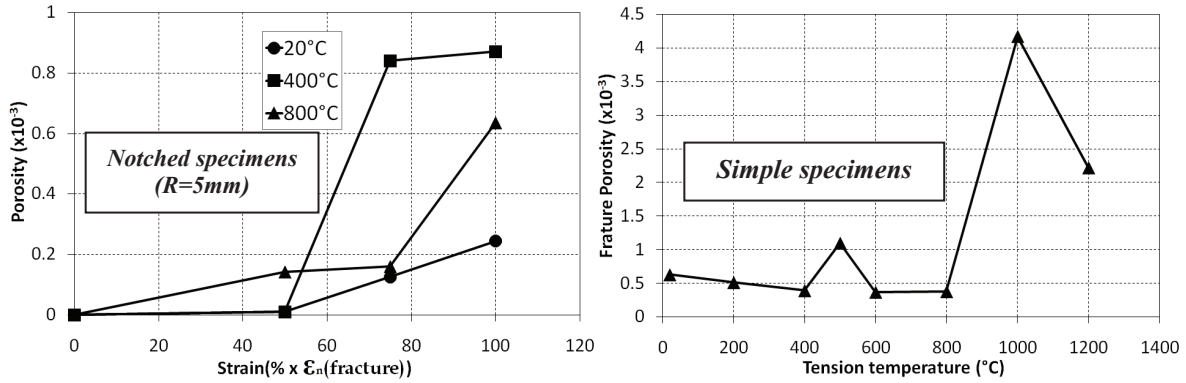

Figure 16: Porosity evolution according to the plastic strain at different temperature (on the left) and the failure porosity according to the temperature (on the right) in the case of 100Cr6 steel

The two materials present the same tendency of porosity evolution curve with the plastic strain or the temperature. However there is a factor 10 between the values of porosity obtained with 42CrMo4 steel and the 100Cr6 steel. This is explained by the fact why the damage mechanism of the 42CrMo4 authorizes relatively high values of porosity. Indeed the frequent presence of manganese sulphide inclusions with considerable size, which without exception damage all what makes increase the proportion of voids. In the case of 100Cr6 steel, the size of carbides is slightly, in more the break is not total but occasional what cause a drop in the proportion of voids.

4.5 The triaxiality degree effect

The localized damage models introduce generally this parameter in various methods. The increase in this parameter, which is equal to 1/3 in the case of uniaxial tensile, decreases the total strain due to the fracture. We notice that the maximum stress increases too.

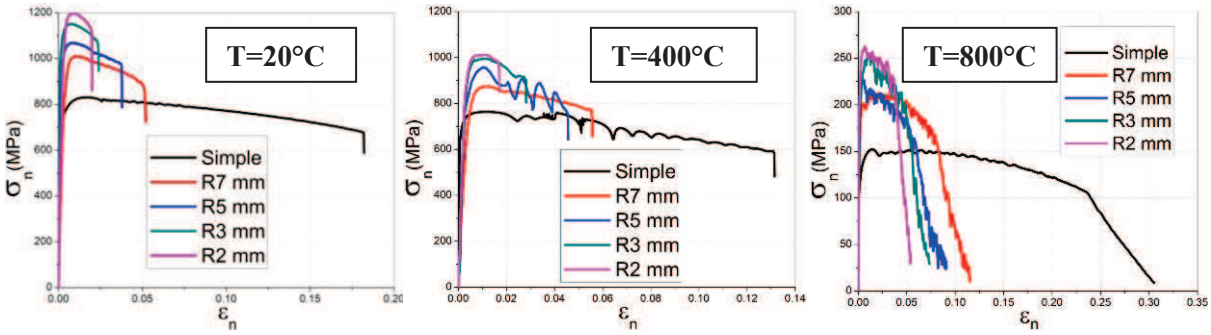

Figure 17: Nominal stress-total strain Curves for temperatures 20, 400 and 800 °C and various triaxiality degree in the case of 42CrMo4 steel

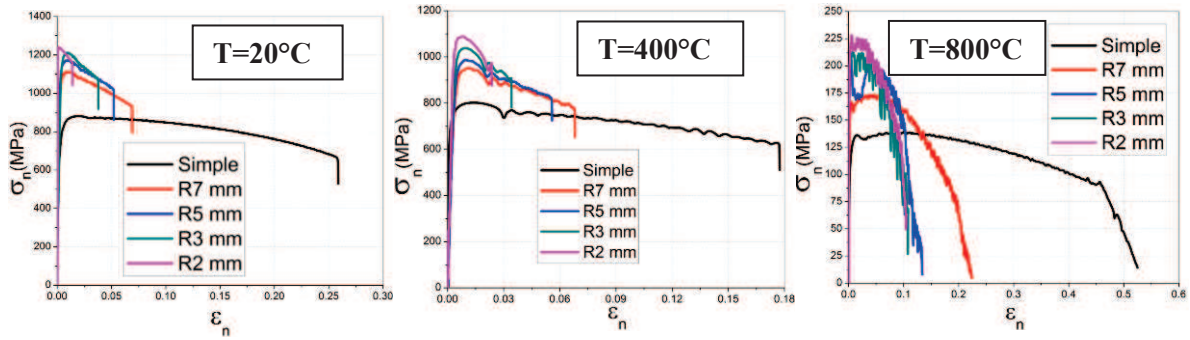

Figure 18: Nominal stress-total strain Curves for temperatures 20, 400 and 800 °C and various triaxiality degree in the case of 100Cr6 steel

5 CONCLUSIONS

- Two steels present different damage mechanisms. Indeed the 42CrMo4 damage by break of manganese sulphide inclusions which introduce with an intergranular rupture, the mechanism of growth is single but a coalescence phenomenon is very random. The 100Cr6 very early damages by the break carbon and chromium carbide which multiplies and believes until the rupture. These mechanisms were observed on the surface and in volume for two materials (figure 19).
- The values of porosity are low in the case of the 100Cr6 steel and higher in the case of 42CrMo4 steel.
- The effect of triaxiality degree is the same for two steel.
- This study will be completed thereafter by the direct and inverse identification and qualification of the damage models based on the theory of local fracture.

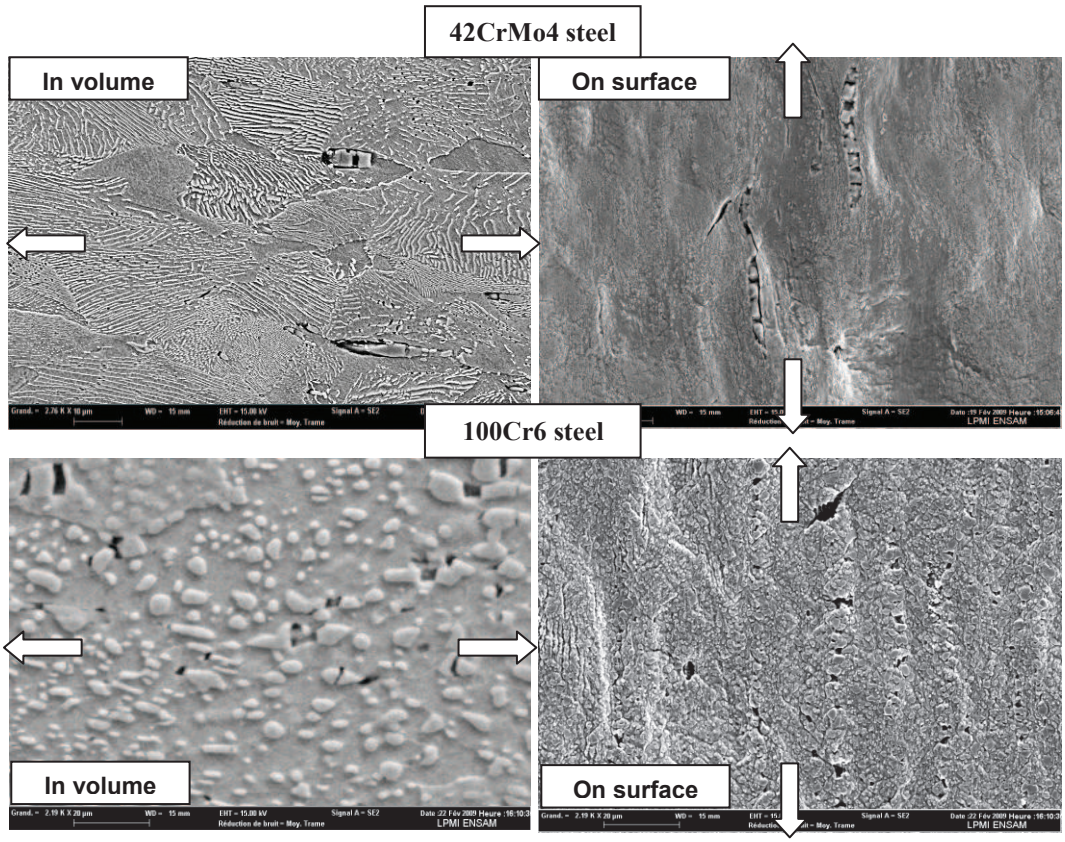

Figure 19: Damage mechanisms on the surface and volume of two steels 100Cr6 and 42CrMo4

REFERENCES

[1] C. Geney, *Etude expérimentale et modélisation par approche locale de la rupture ductile de trois aciers inoxydables austénitiques et d'un acier 16MnD5*. Ecole Centrale de Lille PhD, 1998.

[2] M. Gologanu, *Etude de quelques problèmes de rupture ductile des métaux*. PARIS 6 University PhD, 1997.

[3] J.R. Rice, D.M. Tracey, Journal of the Mechanics and Physics of Solids Vol 17, 201-217, 1969.

[4] A.L. Gurson, *Continuum theory of ductile rupture by void nucleation and growth: Part I-Yield criteria and flow rules for porous ductile media*. J. Engng. Mater. Tech., Vol 99, 147-169, 1977.

[5] G. Rousselier, *Finite deformation constituve relations including ductile fracture damage*. Three-Dimensional Constitutive Relations and Ductile Fracture, North-Holland Pub. Comp., 331-355, 1981.

[6] F. Hild and S. Roux, CORRELI^{Q4}: *Software for "Finite-element" Displacement Field Measurements by Digital Image Correlation*. ENS de Cachan, CNRS-UMR 8535, Paris 6 university , PRES UniverSud Paris, 2008.

[7] J. Lemaitre and J-L. Chaboche, *Mécanique des matériaux solides*, Dunod, Paris, 1996.

[8] F. Montheillet and F. Moussy, *Physique et mécanique de l'endommagement*, Les éditions de physique, Paris, 1986.